CHEMISTRY
A European Journal

A Journal of
ChemPubSoc Europe

Accepted Article

Title: Syntheses, Properties, and Catalytic Activities of Metal(II) Complexes and Free Bases of Redox-Switchable 20π, 19π, and 18π 5,10,15,20-Tetraaryl-5,15-diazaporphyrinoids

Authors: Keisuke Sudoh, Takaharu Satoh, Toru Amaya, Ko Furukawa, Mao Minoura, Haruyuki Nakano, and Yoshihiro Matano

To be cited as: *Chem. Eur. J.* 10.1002/chem.201703664

Link to VoR: http://dx.doi.org/10.1002/chem.201703664

Supported by
ACES

WILEY-VCH

10.1002/chem.201703664

WILEY-VCH

Syntheses, Properties, and Catalytic Activities of Metal(II) Complexes and Free Bases of Redox-Switchable 20π, 19π, and 18π 5,10,15,20-Tetraaryl-5,15-diazaporphyrinoids

Keisuke Sudoh,[b] Takaharu Satoh,[b] Toru Amaya,*[c] Ko Furukawa,*[d] Mao Minoura,[e] Haruyuki Nakano,[f] and Yoshihiro Matano*[a]

Dedication ((optional))

Abstract: In spite of significant advances in redox-active porphyrin-based materials and catalysts, little attention has been paid to 20π and 19π porphyrins, because of their instability in air. Here we report the *meso*-modification of 5,10,15,20-tetraarylporphyrin with two nitrogen atoms, which led to redox-switchable 20π, 19π, and 18π 5,10,15,20-tetraaryl-5,15-diazaporphyrinoids (TADAPs). Three kinds of metal(II) complexes and free bases of TADAP were prepared by the metal-templated annulation of the corresponding metal–bis(dipyrrin) complexes. The inductive and resonance effects of the *meso*-nitrogen atoms on the aromatic, optical, electrochemical, and magnetic properties of the entire TADAP π-systems were assessed, using various spectroscopic measurements and density functional theory calculations. The aromaticity and π–π* electronic transition energies of the TADAPs varied considerably, depending on the oxidation states of the π-systems. The 20π and 19π TADAPs were chemically stable under air, in contrast to the isoelectronic 5,10,15,20-tetraarylporphyrin derivatives. In particular, the 19π TADAP radical cations were extremely stable towards dioxygen, moisture, and silica gel. This reflected the low-lying singly occupied molecular orbitals of their π-systems, and the efficient delocalization of their unshared electron spin. The capability of MgTADAP to catalyze aerobic biaryl formation from aryl Grignard reagents was demonstrated, which presumably involved a 19π–20π redox cycle.

[a] Prof. Dr. Y. Matano
Department of Chemistry, Faculty of Science,
Niigata University, Nishi-ku, Niigata 950-2181 (Japan)
E-mail: matano@chem.sc.niigata-u.ac.jp
[b] K. Sudoh, T. Satoh
Department of Fundamental Sciences, Graduate School of Science and Technology,
Niigata University, Nishi-ku, Niigata 950-2181 (Japan)
[c] Prof. Dr. T. Amaya
Department of Applied Chemistry, Graduate School of Engineering,
Osaka University, Suita, Osaka 565-0871 (Japan)
E-mail: amaya@chem.eng.osaka-u.ac.jp
[d] Prof. Dr. K. Furukawa
Center for Coordination of Research Facilities, Institute for Research Promotion, Niigata University, Nishi-ku, Niigata 950-2181 (Japan)
E-mail: kou-f@chem.sc.niigata-u.ac.jp
[e] Prof. Dr. M. Minoura
Department of Chemistry, College of Science,
Rikkyo University, Toshima-ku, Tokyo 171-8501 (Japan)
[f] Prof. Dr. H. Nakano
Department of Chemistry, Graduate School of Science,
Kyushu University, Nishi-ku, Fukuoka 819-0395 (Japan)

Supporting information (including experimental details) and the ORCID identification numbers for the authors of this article can be found under http://dx.doi.org/10.1002/XXXX.

Introduction

Porphyrins are well known as redox-active macrocyclic ligands and 18π-electron aromatic molecules. The redox properties of porphyrins control a variety of electron/energy transfer processes in nature and industry. There is therefore considerable interest in the aromatic, optical, and magnetic properties of the resulting oxidized/reduced macrocyclic π-systems.[1,2] One-electron and two-electron reductions of a neutral 18π porphyrin ring produce the 19π radical anion and 20π dianion, respectively. In general, these anionic porphyrins are extremely air sensitive because of their high-lying singly occupied molecular orbital (SOMO) and highest occupied molecular orbital (HOMO). Such sensitivity hampers their isolation and characterization in air. Three strategies for isolating 20π porphyrins in neutral form have so far been reported; modification of the core nitrogen atoms (core modification), metal complexation at the core, and peripheral substitution with appropriate functional groups.[3–13] Selected examples prepared according to these strategies are shown in Chart 1. Vogel and co-workers reported the first examples of core-modified 20π porphyrins (isophlorins) **P1** and tetraoxaisophlorin.[3] Similarly, *N*-alkyl-,[4] O-,[5] S-,[6] O,N-,[7] O,S-,[5] and P,S-containing[8] isophlorins have been reported by other groups. Vaid and co-workers synthesized six-coordinate silicon(IV) and germanium(IV) complexes of 5,10,15,20-tetraphenylporphyrin (TPP) **P2**[9] and phthalocyanine,[10] in which the N_4-macrocycles were coordinated to the metal center as −4 ligands with 20π-electrons. Brothers et al. used the same strategy to obtain the 20π TPP-type porphyrin by inserting a diboron (B_2^{4+}) unit into the core.[11] We reported the combined use of core modification and metal complexation to obtain the air stable palladium(II) complex of P,S,N_2-isophlorin.[12] Chen et al. isolated the free base of isophlorin **P3** by appending four trifluoromethyl and four phenyl groups at the periphery of the porphyrin.[13] However, these approaches often cause severe distortion of the 20π framework because of steric repulsion of the substituents at the core or periphery. This distortion impedes a comprehensive understanding of properties associated with the 20π–18π redox processes. Kobayashi et al. reported the first synthesis of an air-stable 19π tetraazaporphyrin **P4**, which included a six-coordinate phosphorus(V) atom at the core.[14] However, to our knowledge there have been few reported air-stable 19π porphyrins and their potential as redox-active catalysts and materials has not yet

been elucidated. Developing a conceptually new molecular design for precisely tuning the redox properties of porphyrin-based 19π and 20π-systems is a challenge, both from fundamentally and from an application perspective.

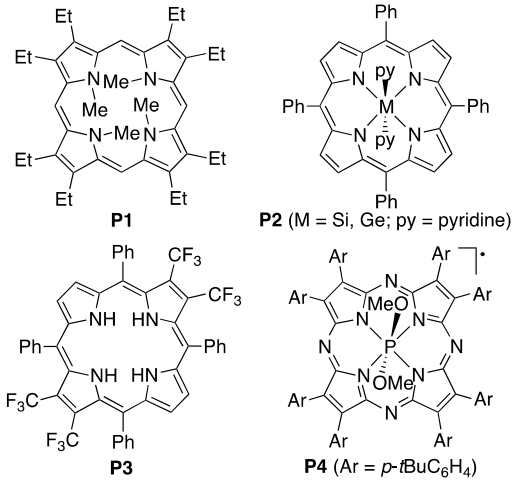

Chart 1. Selected examples of 20π and 19π porphyrins.

It is well known that partial replacement of the *meso*-methine (CR; R = H, aryl, etc.) units of a porphyrin with nitrogen atoms lowers its molecular symmetry, and stabilizes the HOMO and lowest unoccupied molecular orbital (LUMO) energies of its π-system. For example, the redox properties of 5,15-diazaporphyrins (DAPs) differ substantially from those of their porphyrin counterparts;[15–17] DAPs are less readily oxidized and more readily reduced than porphyrins. By contrast, little attention has been paid to the *meso* modification of porphyrins with amine (NR) units. We envisioned that replacing two CR units at the 5 and 15 positions of TPP-type porphyrins with two NR units would be a promising strategy for obtaining redox-switchable 20π, 19π, and 18π azaporphyrins (Scheme 1). Our design concept is based on the idea that the unshared electron pairs of the two *meso*-N atoms would be involved in the π-circuit, and alter its net charge for two electrons. Thus, 5,10,15,20-tetraaryl-5,15-diaza-5,15-dihydroporphyrin (TADAP) **1M**, its radical cation ($TADAP^{•+}$) **2M**, and its dication ($TADAP^{2+}$) **3M** would be isoelectronic forms of 20π TPP^{2-}, 19π $TPP^{•-}$, and 18π TPP, respectively. The net charges of these TADAP π-systems are more positive than those of the parent porphyrin π-systems, implying that the 20π and 19π TADAP derivatives would be more resistant to oxidation than their porphyrin counterparts. This concept was demonstrated in the first syntheses of 20π, 19π, and 18π nickel(II) complexes of TADAP derivatives (NiTADAPs).[18] All NiTADAPs are isolable as air-stable solids, and exhibit reversible redox processes among the 20π–19π–18π oxidation states. Shinokubo and co-workers independently reported the synthesis of the nickel(II) complex and free base of 20π 10,20-diaryl-5,15-diaza-5,15-dihydroporphyrin from the corresponding 18π DAPs.[19] However, these *meso*-NH derivatives readily underwent dehydrogenative oxidation to regenerate the parent DAPs under air.[20] These findings indicate that N-aryl groups in NiTADAPs provide substantial stability to the three π-systems, **1Ni**, **2Ni**, and **3Ni**. Encouraged by our preliminary results, we decided to investigate the effects of the central metals and *meso*-substituents on the fundamental properties of TADAP π-systems. We anticipated that a precisely designed TADAP could be used as a redox-active catalyst for the oxidative coupling of organomagnesium compounds under molecular oxygen as a terminal oxidant, which is challenging because a possible side reaction of the organomagnesium compounds with molecular oxygen makes this reaction more complicated.[21] Herein, we report our comprehensive study of three kinds of metal(II) complexes and free bases of 20π, 19π, and 18π TADAPs. The syntheses and aromatic, optical, electrochemical, and magnetic properties of the TADAPs are discussed based on both experimental and theoretical results. Preliminary results on the catalytic application of TADAP in the oxidative homo-coupling of organomagnesium compounds are also reported.

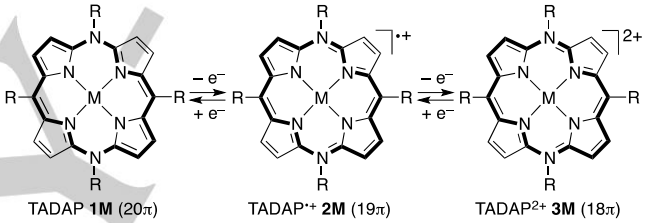

Scheme 1. Interconversion among three oxidation states of TADAP.

Results and Discussion

Synthesis. Scheme 2 illustrates the syntheses of zinc(II) complexes of TADAP derivatives (ZnTADAPs). Treatment of 3-chloro-5-arylamino-8-mesityldipyrrins **4a**–**d** (mesityl = 2,4,6-trimethylphenyl) with a half equiv. of zinc(II) acetate afforded the corresponding zinc(II)–bis(dipyrrin) complexes **5Zn-a**–**d**. When the Zn-templated annulation reaction of **5Zn-a** was conducted using K_2CO_3 and DMF, which were used in the synthesis of NiTADAPs,[18] the desired 20π ZnTADAP **1Zn-a** was formed in low yield because of the partial demetalation of **5Zn-a**. When NaO*t*Bu and toluene were used instead of K_2CO_3 and DMF, the expected annulation, namely intramolecular double nucleophilic substitution reaction of **5Zn-a** occurred smoothly to afford **1Zn-a**. Similarly, **1Zn-b**–**d** were obtained from **5Zn-b**–**d**. The almost exclusive formation of **1Zn** from **5Zn** was confirmed by NMR spectroscopy and high-resolution mass (HRMS) spectrometry. However, **1Zn-a**–**d** were slowly oxidized in solution in the presence of air. Therefore, crude **1Zn-a**–**d** were subsequently oxidized to 18π $ZnTADAP^{2+}$ **3Zn-a**–**d**, by treatment with 2 equiv. of $AgPF_6$. Dications **3Zn** were isolated as purple solids, by recrystallization from CH_2Cl_2–Et_2O. The one-electron reduction of **3Zn-a**–**d** with $NaBH_4$ or bis(cyclopentadienyl)cobalt(II) ($CoCp_2$) at room temperature afforded the corresponding 19π $ZnTADAP^{•+}$ **2Zn-a**–**d**, which were isolated as greenish yellow

solids by silica-gel column chromatography and subsequent recrystallization from CH_2Cl_2–hexane.

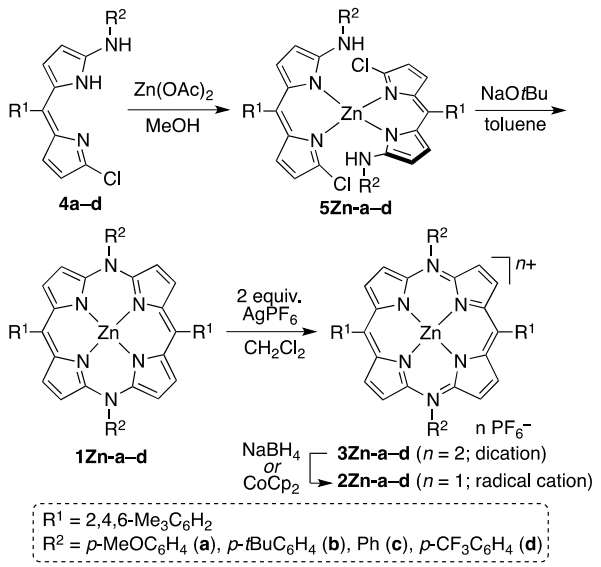

Scheme 2. Synthesis of ZnTADAPs.

We next applied a metal-templated annulation method to synthesize copper(II) complexes of the TADAP derivatives (CuTADAPs). When **4b** was treated with a half equiv. of copper(II) acetate in CH_2Cl_2–MeOH, 19π CuTADAP$^{•+}$ **2Cu'-b** was unexpectedly obtained in moderate yield instead of the copper(II)–bis(dipyrrin) complex **5Cu-b** (Scheme 3). The copper(II) salt most likely promoted the intramolecular N–C coupling of **5Cu-b**, but then also oxidized the resulting 20π CuTADAP. Indeed, when **4b** was treated with 1.2 equiv. of copper(II) acetate, **2Cu'-b** was isolated in better yield. Similarly, **2Cu'-a**,**d** were directly formed from **4a**,**d** and copper(II) acetate. At this stage, the counter anions of **2Cu'** were not characterized, and **2Cu'** were reduced to 20π CuTADAP **1Cu** by treatment with $NaBH_4$. Oxidation of **1Cu-a**,**b**,**d** with 2 equiv. of $AgPF_6$ afforded the corresponding 18π CuTADAP^{2+} **3Cu-a**,**b**,**d**, after reprecipitation from CH_2Cl_2–Et_2O. Furthermore, the mixing of equimolar amounts of **1Cu** and **3Cu** in CH_2Cl_2 quantitatively produced 19π CuTADAP$^{•+}$ **2Cu-a**,**b**,**d** as hexafluorophosphates. In this anti-disproportionation reaction, single electron transfer from **1Cu** to **3Cu** occurred to form two moles of **2Cu**.

Free bases of TADAP derivatives (H_2TADAPs) were not afforded by the acidolysis of **2Zn** and **3Zn**, which remained intact after prolonged treatment with CF_3CO_2H. Therefore, we used the Yorimitsu–Osuka procedure for the two-step transformation of metalloporphyrins to free bases via magnesium(II) porphyrins;[22] step one was exchange of the central metal from Ni/Zn/Cu/Ag to Mg, by treatment with a Grignard reagent; step two was acidolysis. After screening reaction conditions, we obtained H_2TADAP in moderate yield starting from **2Zn-a** (Scheme 4). The addition of 60 equiv. of phenylmagnesium bromide (PhMgBr; THF solution) to a toluene solution of **2Zn-a** quickly changed the color from yellow to red. The ^{1}H NMR and HRMS spectra of the reaction mixture were consistent with the formation of the 20π magnesium(II) complex of TADAP (MgTADAP) **1Mg-a**. However, this complex could not be isolated because of its extremely high sensitivity to air (vide infra). After 10 min of stirring under nitrogen atmosphere, the reaction mixture was treated with excess CF_3CO_2H, which cleaved the Mg–N bonds of **1Mg-a** to afford 20π H_2TADAP **1H$_2$-a** in 34% overall yield from **2Zn-a**. Alternatively, **1H$_2$-a** was prepared from **5Zn-a** in a one-pot procedure via **1Zn-a**, which underwent the Zn-to-Mg exchange reaction to give **1Mg-a**. One-electron and two-electron oxidation reactions of **1H$_2$-a** with $AgPF_6$ gave 19π H_2TADAP$^{•+}$ **2H$_2$-a** and 18π H_2TADAP^{2+} **3H$_2$-a**, respectively. New NiTADAPs **1Ni-a**, **2Ni-a**, and **3Ni-a** were prepared according to reported methods.[18] Notably, all of the radical cations **2M** are rare examples of 19π porphyrins with high stability toward dioxygen, moisture, and silica gel.

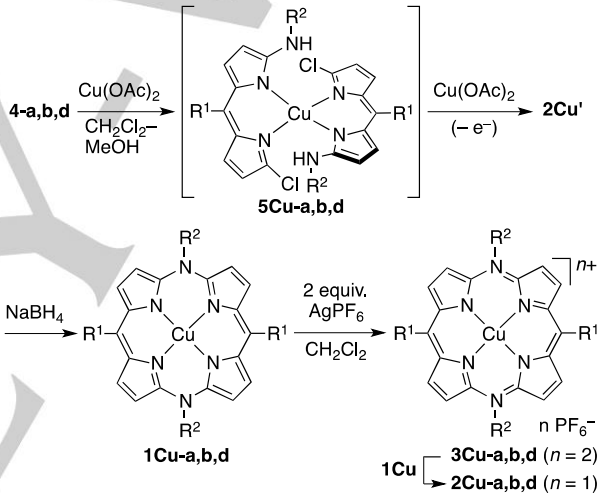

Scheme 3. Synthesis of CuTADAPs.

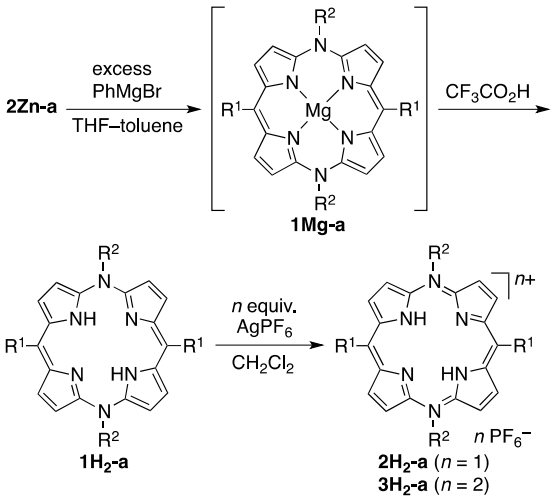

Scheme 4. Synthesis of H_2TADAPs.

Characterization. MTADAPs (M = Zn, Cu, Ni, H_2) were characterized by NMR and IR spectroscopy, HRMS, and X-ray crystallography (for **1Cu-b** and **2Ni-a**). In the HRMS spectra of **1M**, **2M**, and **3M**, intense peaks are detected and are consistent with m/z = $[M]^+$, $[M - PF_6]^+$, and $[M - 2(PF_6)]^{z+}$ (z = 1, 2), respectively. In the $^{31}P\{^1H\}$ NMR spectra of **2M** and **3M** (M = Zn, Ni), a characteristic septet from the hexafluorophosphate ion is observed at δ = −141 to −146 ppm (J_{P-F} = 711 to 713 Hz). Correlation between the ring-current effects in the ^1H NMR spectra and the aromaticity of the 20π and 18π MTADAPs (M = Zn, H_2) is discussed in the following section.

The crystal structures of **1Cu-b** and **2Ni-a** were elucidated by X-ray crystallography.[23] The copper center in **1Cu-b** adopts a square planar geometry, whereas the nickel center in **2Ni-a** adopts an octahedral geometry with two THF-oxygen atoms as the axial ligands. Although the counter anion (PF_6^-) and axial THF molecules of **2Ni-a** showed positional disorder, the TADAP moiety was satisfactorily refined. As shown in Figure 1 and Figure S1 in the Supporting Information (SI), both **1Cu-b** and **2Ni-a** have highly flat DAP π-planes with root-mean-square deviations (d_{rms}) of 0.029 and 0.044 Å, respectively. The *meso*-aryl groups are almost perpendicular to the DAP ring (dihedral angles are 74.0–86.5° for the 10,20-mesityl groups and 82.3–85.4° for the 5,15-aryl groups). This suggests that π-conjugation between the *meso*-aryl groups and the DAP ring is very small. The relatively short C1–N2 and C2–N2 bonds (average bond lengths are 1.381 Å for **1Cu-b** and 1.371 Å for **2Ni-a**) indicate that the unshared electron pairs in the p orbitals of the *meso*-N atoms are effectively conjugated with the π-orbitals in the adjacent α-pyrrolic carbon atoms (Table S1 in SI). The average Cu–N bond length of **1Cu-b** (1.986 Å) is slightly longer than the average Ni–N bond length of **1Ni-b** (1.945 Å),[18] reflecting the different covalent radii of Cu and Ni.

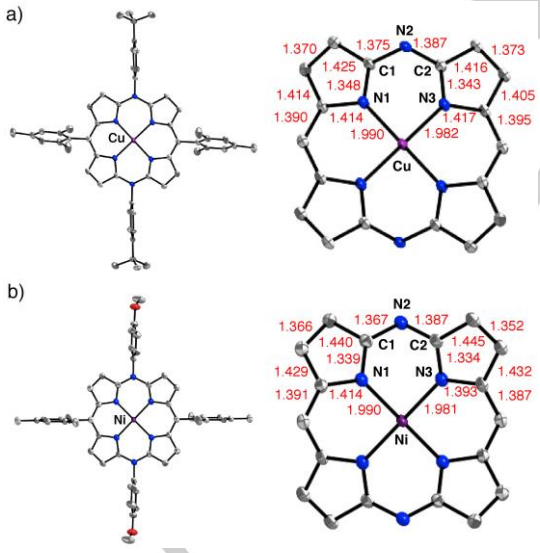

Figure 1. Top views (50% probability ellipsoids) of a) **1Cu-b** and b) **2Ni-a** (a part of two independent crystals). Hydrogen atoms are omitted for clarity. For **2Ni-a**, the counter PF_6^- ion and two axial THF ligands are also omitted. Bond lengths (Å) except the standard deviations (0.001–0.003 Å for **1Cu-b**, 0.002–0.004 Å for **2Ni-a**) are shown in red.

Aromaticity. As mentioned above, the unshared electron pairs of the *meso*-N atoms of TADAP can be involved in the macrocyclic π-circuit. This implies that **1M** and **3M** are isoelectronic with the corresponding metal complexes of the 20π TPP dianion and 18π TPP, respectively. Taking these π-electron counts into consideration, the aromatic character of **1M** and **3M** is discussed. Diatropic and paratropic ring-current effects in the ^1H NMR spectra are a good index for evaluating aromaticity and antiaromaticity, respectively, in terms of a magnetic criterion. Representative ^1H NMR spectra are shown in Figure 2. The peripheral β protons (*d* and *e*) of **1Zn-c** appear at δ = 4.05 and 2.81 ppm in C_6D_6, whereas those of **3Zn-c** appear at δ = 8.64 and 8.25 ppm in CD_2Cl_2. These upfield and downfield shifts of the peripheral protons indicate that **1Zn-c** and **3Zn-c** receive considerable paratropic (20π) and diatropic (18π) ring currents, respectively. The *ortho*-, *meta*-, and *para*-protons of the *meso*-aryl groups (c*, f*, *g*, and *h*) of **1Zn-c** and **3Zn-c** also receive the opposite ring-current effects from each other. Similar spectral features are observed for the other 20π/18π MTADAPs (M = Zn, Ni, H_2). The chemical shifts (in $CDCl_3$ or CD_2Cl_2) of the β protons of **3Zn** (δ = 8.64–8.54, 8.27–8.20 ppm) and **3H₂-a** (δ = 8.64, 8.3 ppm) are shifted upfield compared with the corresponding chemical shifts of the 18π porphyrin references **6Zn** (δ = 8.89, 8.78 ppm) and **6H₂** (δ = 8.78, 8.68 ppm).[24] In contrast, the β protons of **1Zn** (δ = 2.8 to 4.1 ppm) are shifted downfield compared with those of a ZnTPP dianion (δ = −0.9 ppm in $[D_8]$THF).[2d] These differences may be attributed to different charges and electron densities of the entire π-systems between **1Zn/3Zn** and the ZnTPP counterparts (20π dianion/18π neutral molecule). The ^1H NMR spectrum of **1H₂-a** in C_6D_6 displays the inner NH protons at δ = 24.87 ppm (Figure S2 in SI), which is close to the value reported for 10,20-dimesityl-5,15-diaza-5,15-dihydroporphyrin (δ = 24.5 ppm in $[D_8]$THF).[19] The downfield appearance of the NH protons of **3H₂-a** (δ = −0.54 ppm) relative to those of **6H₂** (δ = −2.62 ppm)[24] and **7H₂** (δ = −2.61 ppm)[17b] may reflect a positive charge of the π-system in **3H₂-a**.

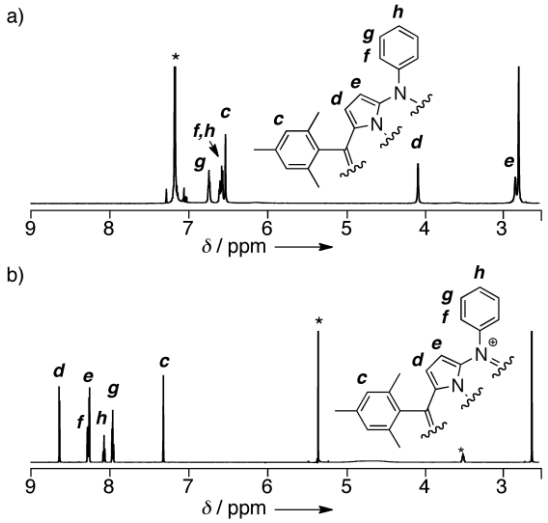

Figure 2. ^1H NMR spectra of a) **1Zn-c** in C_6D_6 and b) **3Zn-c** in CD_2Cl_2. Asterisks indicate residual solvent peaks.

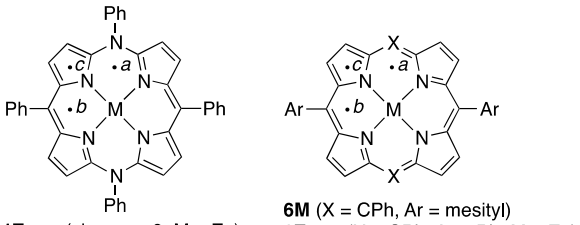

1Zn-m (charge = 0, M = Zn)
2M-m (charge = +1)
3Zn-m (charge = +2, M = Zn)

6M (X = CPh, Ar = mesityl)
6Zn-m (X = CPh, Ar = Ph, M = Zn)
7M (X = N, Ar = mesityl)
7Zn-m (X = N, Ar = Ph, M = Zn)

Chart 2. MTADAP models (**1Zn-m**, **2M-m**, **3Zn-m**), porphyrin references and models (**6M**, **6Zn-m**), and DAP references and models (**7M**, **7Zn-m**).

To gain deeper insight into the ring-current effects of the TADAP π-systems, we calculated nuclear independent chemical shifts (NICS)[25] at three positions in the π-planes of the ZnTADAP models **1Zn-m** and **3Zn-m** (Chart 2). The NICS values at the midpoints between the two adjacent pyrrole rings (*a* and *b*) in **1Zn-m** are +8.13 and +9.32 ppm, respectively, indicating that there are global paratropic ring currents in its 20π circuit. In contrast, the NICS value at the center of the pyrrole ring (*c*) in **1Zn-m** is −6.51 ppm, implying that the pyrrole ring has local diatropic ring currents. The NICS values at the *a*, *b*, and *c* positions in the π-plane of **3Zn-m** are −17.72, −17.11, and −7.06 ppm, respectively, which are apparently due to diatropic ring currents derived from the 18π circuit. As a whole, the DAP π-systems in **1Zn-m** and **3Zn-m** have substantial antiaromatic and aromatic character, respectively, in terms of the ring-current effects. The NICS values of **3Zn-m** are less negative than those of the porphyrin model **6Zn-m** (δ = −18.76 and −9.26 ppm at *a* (= *b*) and *c*, respectively) and DAP model **7Zn-m** (δ = −18.93 and −19.22 ppm at *a* and *b*, respectively). This suggests that the macrocyclic ring-current effects of 18π ZnTADAP are slightly weaker than those of ZnTPP and ZnDAP.

Optical and Redox Properties. Table 1 summarizes the experimentally observed optical data for the MTADAPs and porphyrin/DAP references. The UV/vis/NIR absorption spectra of the 5,15-*p*-anisyl-substituted derivatives **1M-a**, **2M-a**, and **3M-a** (M = Zn, Cu, Ni, H_2) are shown in Figure 3. In a series of metal complexes bearing *p*-anisyl groups, **1M-a** exhibit two intense absorption bands with absorption maxima (λ_{max}) of 444–446 and 519–531 nm, whereas **3M-a** exhibit two intense bands with λ_{max} of 391–393 and 629–632 nm. The λ_{max} of the free bases **1H₂-a** (426 and 488 nm) and **3H₂-a** (390 and 645 nm) differ from those of their metal complexes, as is typically observed for porphyrins. The Q-like bands of **3M-c** (M = Zn, Ni) are largely red-shifted compared with the Q bands of **6M** (λ_{max} = 526–551 nm; M = Zn, Ni) and **7M** (λ_{max} = 571–584 nm; M = Zn, Ni). This indicates that the HOMO–LUMO gaps of the 18π MTADAPs are considerably smaller than those of the isoelectronic porphyrins and DAPs. The radical cations **2M-a** exhibit intense absorption bands in the NIR region (λ_{max} = 860–890 nm) together with two bands in the UV/vis region, highlighting the characteristic optical properties of their 19π systems. In all three kinds of TADAPs, the *para*-substituents of the *meso*-N-aryl groups exert only small influences on the λ_{max} values.

To understand the nature of π–π* electronic excitations of the TADAP π-systems, we carried out time-dependent density functional theory (TD-DFT) calculations on **1Zn-m**, **3Zn-m**, and **6Zn-m** (Figure 4 and Table 2; for the results on nickel(II) complexes, see ref. 18). Both **1Zn-m** and **3Zn-m** have D_2 symmetry, and their HOMO/HOMO−1 and LUMO/LUMO+1 are nondegenerate because of the electronic effects of the two *meso*-N atoms. As shown in Figure 4, the electron distribution of the HOMO of **1Zn-m** largely corresponds to that of the LUMO of **3Zn-m**. This implies that the two electrons in the HOMO of **1Zn** are removed in the oxidation leading to **3Zn**.

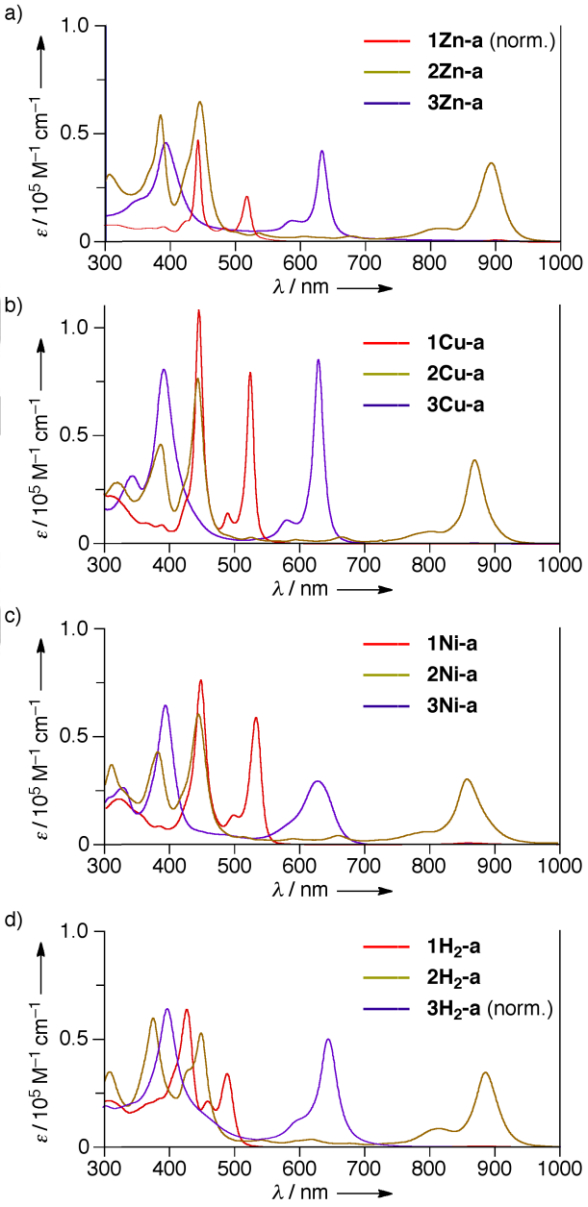

Figure 3. UV/vis/NIR absorption spectra of MTADAPs bearing *p*-anisyl groups: M = Zn (a), Cu (b), Ni (c), and H_2 (d). Measured in CH_2Cl_2. The absorption spectra of **1Zn-a** and **3H₂-a** are normalized to those of **3Zn-a** and **1H₂-a**, respectively, at the absorption maxima.

Table 1. Optical data for MTADAPs and references.

Compound	λ_{abs} [nm] (log ε)[a]
1Zn-a	444 (n.d.), 519 (n.d.)
1Zn-b	445 (n.d.), 519 (n.d.)
1Zn-c	443 (n.d.), 518 (n.d.)
1Zn-d	443 (n.d.), 516 (n.d.)
1Cu-a	444 (5.05), 522 (4.87)
1Cu-b	444 (5.06), 523 (4.87)
1Cu-d	443 (5.09), 519 (4.94)
1Ni-a	446 (4.89), 531 (4.78)
1Ni-b	446 (4.96), 532 (4.85) [b]
1Ni-c	445 (4.94), 531 (4.81) [b]
1H$_2$-a	426 (4.80), 488 (4.53)
2Zn-a	384 (4.73), 448 (4.81), 890 (4.54)
2Zn-b	385 (4.79), 447 (4.90), 890 (4.63)
2Zn-c	384 (4.77), 445 (4.81), 894 (4.56)
2Zn-d	382 (4.79), 442 (4.85), 903 (4.55)
2Cu-a	384 (4.70), 444 (4.82), 871 (4.59)
2Cu-b	387 (4.66), 444 (4.88), 870 (4.59)
2Cu-d	384 (4.70), 440 (4.87), 879 (4.60)
2Ni-a	381 (4.63), 444 (4.78), 860 (4.47)
2Ni-b	384 (4.56), 444 (4.80), 860 (4.43) [b]
2H$_2$-a	375 (4.77), 449 (4.71), 888 (4.53)
3Zn-a	389 (4.76), 634 (4.63)
3Zn-b	388 (4.95), 634 (4.93)
3Zn-c	392 (4.66), 632 (4.65)
3Zn-d	391 (4.88), 634 (4.77)
3Cu-a	392 (4.95), 631 (4.85)
3Cu-b	391 (4.91), 630 (4.93)
3Cu-d	394 (4.85), 628 (4.72)
3Ni-a	393 (4.81), 629 (4.47)
3Ni-b	393 (4.82), 627 (4.55) [b]
3Ni-c	397 (4.78), 626 (4.51) [b]
3H$_2$-a	390 (n.d.), 645 (n.d.)
6Zn	421 (5.67), 551 (4.26)
6Ni	413 (5.29), 526 (4.15) [b]
7Zn	394 (4.92), 584 (4.86) [c]
7Cu	384 (4.98), 397 (4.97), 577 (4.94) [c]
7Ni	373 (4.79), 390 (4.89), 571 (4.78) [c]
7H$_2$	393 (5.11), 541 (4.51), 627 (4.62) [c]

[a] Measured in CH_2Cl_2. λ_{max} >350 nm and log ε > 4 are listed. R^2 = *p*-$MeOC_6H_4$ (**a**), *p*-$tBuC_6H_4$ (**b**), Ph (**c**), *p*-$CF_3C_6H_4$ (**d**). n.d. = not determined. [b] Data from ref. 18. [c] Data from ref. 17.

The orbital characteristics and energies of **3Zn-m** differ considerably from those of **6Zn-m**, whose HOMO/HOMO−1 and LUMO/LUMO+1 are intrinsically degenerate and are located at high-lying energy levels because of the neutral, D_4-symmetric π-system. From the results of the TD-DFT calculations, the longest-wavelength bands observed for **1Zn** are assigned to a combination of the HOMO-to-LUMO+1 and HOMO−1-to-LUMO excitations, whereas those observed for **3Zn** are assigned to the essential HOMO-to-LUMO excitation. The TD-DFT results also clarify that the HOMO-to-LUMO excitation of **1Zn-m** is symmetrically forbidden (oscillator strength ~ 0).

The 18π ZnTADAP^{2+} **3Zn** and H_2TADAP^{2+} **3H$_2$-a** are weakly fluorescent in CH_2Cl_2 (Figure S3 in SI). The optical HOMO–LUMO gaps of **3Zn-a** and **3H$_2$-a** (1.94 and 1.92 eV, respectively), as estimated from the intersections of the absorption and fluorescence spectra, are considerably smaller than those of the analogous porphyrin **6Zn** and DAPs **7M** (M = Zn, H_2). Accordingly, the 18π TADAPs would be promising frameworks for cationic sensitizers that are capable of responding to long-wavelength visible light.

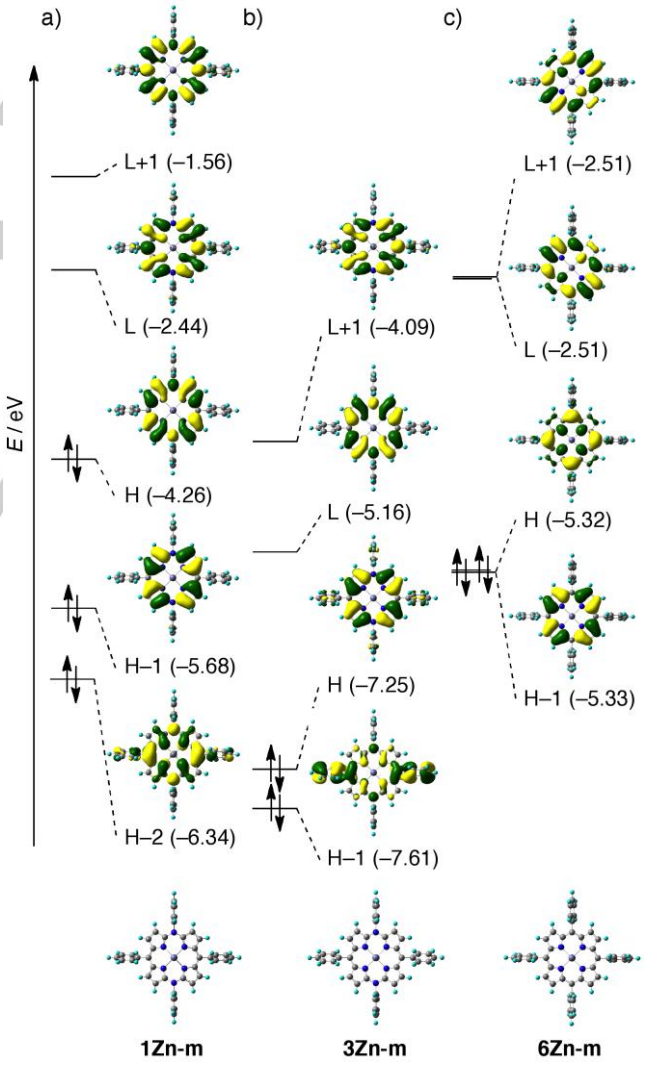

Figure 4. Optimized structures and selected Kohn-Sham orbitals and their energies (in eV) calculated by the DFT method with the solvent effect (PCM, CH_2Cl_2): a) **1Zn-m**, b) **3Zn-m**, and c) **6Zn-m**. H = HOMO; L = LUMO.

Table 2. Excitation energies and oscillator strengths of **1Zn-m**, **3Zn-m**, and **6Zn-m** calculated by the TD-DFT method.[a]

State	Excitation energy [eV/nm]	Oscillator strength (*f*)	Excitation	Weight [%]
1Zn-m				
2	2.41/515	0.166	HOMO → LUMO+1	75.5
			HOMO−1 → LUMO	24.5
6	3.15/394	1.583	HOMO−1 → LUMO	72.0
			HOMO → LUMO+1	23.6
11	3.40/365	0.149	HOMO−5 → LUMO	61.0
			HOMO−2 → LUMO	26.8
13	3.54/351	0.479	HOMO−2 → LUMO	61.3
			HOMO−5 → LUMO	32.0
3Zn-m				
2	2.01/616	0.393	HOMO → LUMO	90.3
16	3.07/404	0.599	HOMO −1→ LUMO+1	89.5
17	3.19/389	0.305	HOMO−4 → LUMO+1	61.0
20	3.37/368	1.241	HOMO−4 → LUMO+1	35.3
			HOMO → LUMO	27.8
6Zn-m				
1	2.28/544	0.013	HOMO → LUMO+1	49.8
			HOMO−1 → LUMO	49.8
3	3.12/398	1.619	HOMO−1 → LUMO	49.4
			HOMO → LUMO	49.4

[a] B3LYP/6-311G(d,p) and Wachters–Hay(f) (PCM, CH_2Cl_2) at the optimized structures. Except for the lowest-energy excited state of **6Zn-m**, the states whose oscillator strengths are less than 0.1 are not included.

Redox potentials of the MTADAPs were measured by cyclic voltammetry in CH_2Cl_2 or THF, with Bu_4NPF_6 as a supporting electrolyte. Selected voltammograms are shown in Figure 5. Regardless of the starting materials (**1M**, **2M**, or **3M**), all the MTADAPs exhibit two reversible redox processes, attributable to 20π/19π and 19π/18π, in the range −0.7 to +1.0 V vs. Ag/Ag^+. For example, MTADAPs bearing the *p*-anisyl groups are oxidized/reduced in two separate one-electron steps at −0.58 and +0.15 V for ZnTADAP, −0.36 and +0.31 V for CuTADAP, −0.37 and +0.29 V for NiTADAP, and −0.19 and +0.44 V for H_2TADAP, respectively (Figure 5a). Both the 20π/19π and 19π/18π redox processes of ZnTADAP occur at more negative potentials than those of NiTADAP and CuTADAP, reflecting the smaller electronegativity of zinc (1.65, Pauling scale) compared with those of copper (1.90) and nickel (1.91). The more negative redox potentials observed for the 20π/19π process of ZnTADAP explains the relatively low stability of **1Zn** in air. However, the 20π/19π redox processes of the MTADAPs occur at much more positive potentials than those of the isoelectronic MTPP dianions (E < −2 V vs Ag/Ag^+). Therefore, it can be concluded that the high stability of **1M** arise from the neutral charge of their 20π-systems.[2d] It should also be noted that the electron-accepting ability of **3M** is considerably higher than that of **6M** [e.g. E(18π/19π) = +0.30 V for **3Ni-c** and −1.69 V for **6Ni-c**, vs. Ag/Ag^+]. The 21π/20π and 20π/19π redox processes of **1Cu-b** in THF are observed at −1.88 and −0.33 V, respectively, vs. Ag/Ag^+ (Figure S4 in SI). From these values, the electrochemical HOMO–LUMO gap of **1Cu-b** is determined to be 1.55 eV.

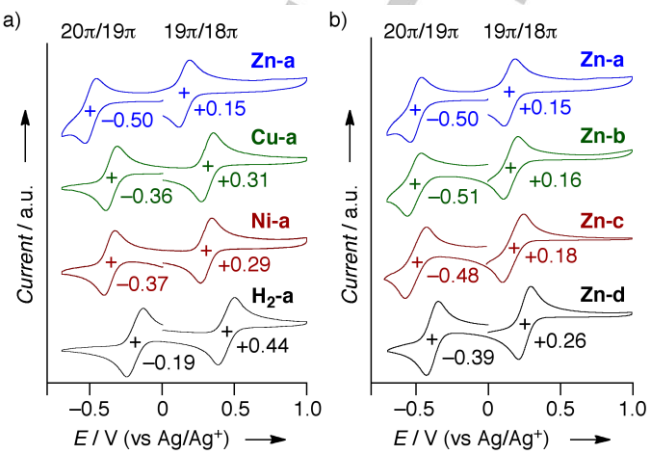

Figure 5. Cyclic voltammograms of a) MTADAPs bearing *N*-*p*-anisyl groups (M = Zn, Cu, Ni, H_2) and b) ZnTADAPs (**a**–**b** denote *para*-substituents of the *N*-aryl groups). Measured in CH_2Cl_2 (from −0.7 to +1.0 V vs. Ag/Ag^+); $Bu_4N^+PF_6^-$ (0.1 M) as a supporting electrolyte; Ag/Ag^+ [$AgNO_3$ (MeCN)] as a reference electrode; scan rate = 60 mV s^{-1}.

The electronic effects of the *para*-substituents of the *N*-aryl groups on the redox potentials of ZnTADAPs are compared in Figure 5b. Introducing an electron-donating group (OMe, *t*Bu) slightly shifts the 20π/19π and 19π/18π processes towards negative potentials (ΔE = −0.02 to −0.03 V; **Zn-a**,**b** vs. **Zn-c**), whereas introducing an electron-withdrawing CF_3 group shifts them towards positive potentials (ΔE = +0.08 to +0.09 V; **Zn-d** vs. **Zn-c**). In all the metal complexes, the *para*-substituents exert small but clear influences on the HOMO and LUMO levels of the π-systems (Table 3).

Table 3. Redox Potentials for MTADAPs.

M	a	b	c	d
Zn	−0.50, +0.15	−0.51, +0.16	−0.48, +0.18	−0.39, +0.26
Cu	−0.36, +0.31	−0.41, +0.27	n.p.	−0.29, +0.32
Ni	−0.37, +0.29	−0.39, +0.30	−0.37, +0.30	n.p.
H_2	−0.19, +0.44	n.p.	n.p.	n.p.

[a] Half-wave potentials (vs. Ag/Ag^+) measured by CV in CH_2Cl_2 with $Bu_4N^+PF_6^-$ (0.1 M). n.p. = not prepared.

Magnetic properties. As mentioned in the Introduction, there are currently few reported air-stable 19π porphyrins. To understand the key factors providing the remarkable stability to the present 19π radical cations, we measured EPR spectra of **2Zn-a**–**d**, **2H$_2$-a**, **1Cu-a**, and **3Cu-a**. The EPR spectrum of **2Ni-c** has been reported previously.[18] As shown in Figure 6a, **2Zn-a** exhibits an EPR signal at g = 2.0039, with the fine structure

derived from two *meso*-^{14}N and four β-^{1}H atoms. The calculated spin distribution of its model **2Zn-m** supports the observed fine structure (Figure 6b).

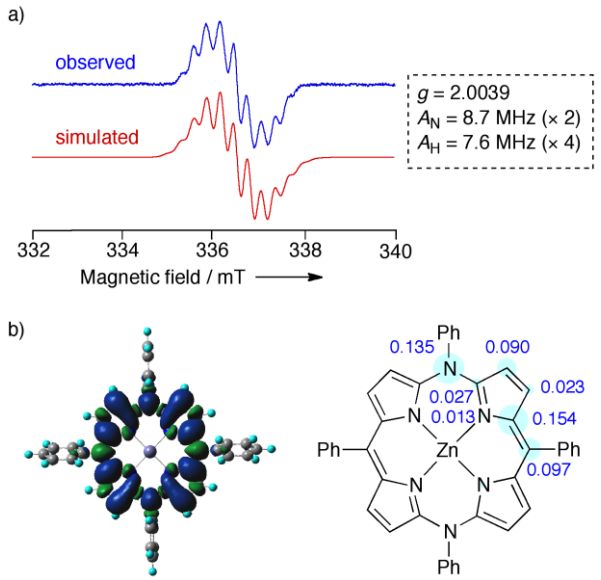

Figure 6. a) EPR spectra of **2Zn-a** observed in toluene (blue) and simulated (red). b) Spin density distribution at the optimized structure (left) and spin densities at the DAP ring (right) of **2Zn-m**: calculated by the DFT method.

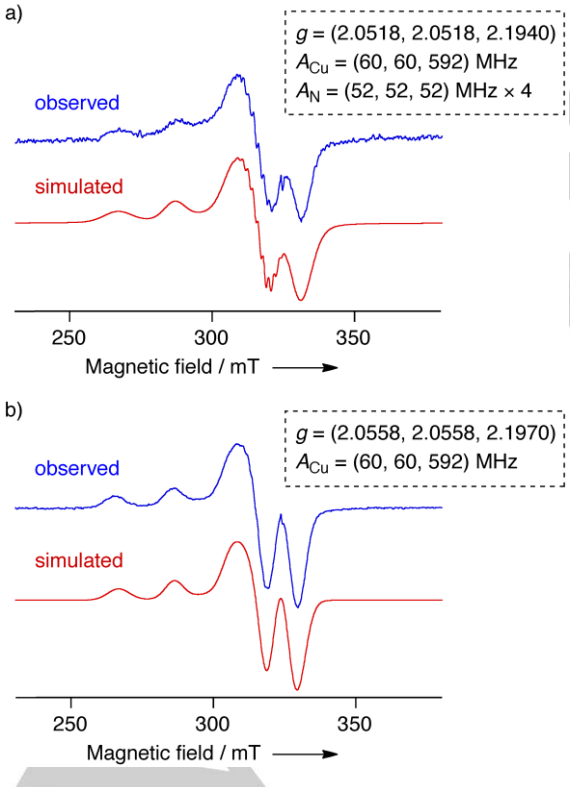

Figure 7. EPR spectra of a) **1Cu-a** and b) **3Cu-a** observed in CH_2Cl_2 at 30 K (blue) and simulated (red).

The other zinc(II) complexes **2Zn-b–d** exhibit similar EPR spectra, featuring small electronic effects of their *para*-substituents on the electron spin distribution (Figure S5 in SI). The free base **2H$_2$-a** exhibits an EPR spectrum at g = 2.0023, with the fine structure derived from *meso*-^{14}N and β-^{1}H atoms (Figure S6 in SI). Most importantly, the unshared electron spin of these 19π radical cations is efficiently delocalized over the entire DAP ring. The aryl groups attached to the *meso*-N/C atoms, which have moderate spin densities, may also contribute to the stabilization of the π-radicals by steric protection. The CuTADAPs **1Cu-a** and **3Cu-a** exhibit EPR signals that are characteristic of related copper(II) (diaza)porphyrins.[26,27] Specifically, the fine structures originating from the d^9 copper center and four core ^{14}N atoms (for **1Cu-a**) are observed at 30 K (Figure 7). These results clearly support that the oxidation state (+2) of the copper center does not change during the redox conversion between **1Cu** and **3Cu**.[28]

TADAP-catalyzed oxidative homo-coupling reactions. As mentioned above, **2Zn-a** was transformed to **1Mg-a** by treatment with excess PhMgBr, whereas **1Mg-a** was quickly converted to **2Mg-a** (the counter anion was not characterized) in air. These results indicate that (1) 19π MTADAP$^{\bullet+}$ can accept one electron from organomagnesium compounds, in view of the redox potential,[29] to become the 20π MTADAP, and (2) 20π MgTADAP is readily oxidized by molecular oxygen to regenerate 19π MgTADAP$^{\bullet+}$.

With these reactivities in mind, we examined a catalytic oxidative homo-coupling of PhMgBr under molecular oxygen to explore the possibility of MTADAP as a redox-active catalyst. The reaction progress was monitored by ^{1}H NMR and EPR spectroscopies (Figure 8) and MALDI-TOF-MS spectrometry. Treatment of **2Zn-a** (19π) with PhMgBr in [D$_8$]THF under nitrogen atmosphere at room temperature stoichiometrically afforded the desired coupling product, biphenyl, together with **1Zn-a** (20π: δ = 3.73 and 2.74 ppm for β-H) and **1Mg-a** (20π: δ = 3.80 and 2.84 ppm for β-H) (Figure 8a).[30] Further addition of PhMgBr induced the complete substitution of Zn^{II} to Mg^{II} in TADAP, forming **1Mg-a** as the major TADAP species (Figure 8b). These observations clearly show that the oxidative homo-coupling of PhMgBr is faster than the metal exchange reaction. Introducing molecular oxygen to this mixture resulted in the disappearance of the peaks of **1Mg-a**, and growth of the peaks of biphenyl and a small amount of a phenol derivative, in the ^{1}H NMR spectrum (Figure 8c). In addition, the EPR and MALDI-TOF-MS spectra of the resulting mixture show the generation of **2Mg-a** (19π, g = 2.003). Again, a sequence of the addition of PhMgBr followed by exposure to molecular oxygen was repeated. This resulted in similar behavior in the ^{1}H NMR and EPR spectra (Figure 8d,e), clearly showing the catalytic cycle of 20π/19π MgTADAP (Scheme 5).[31]

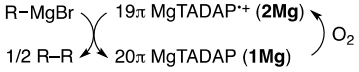

Scheme 5. Plausible catalytic cycle for MgTADAP-catalyzed oxidative homo-coupling reaction.

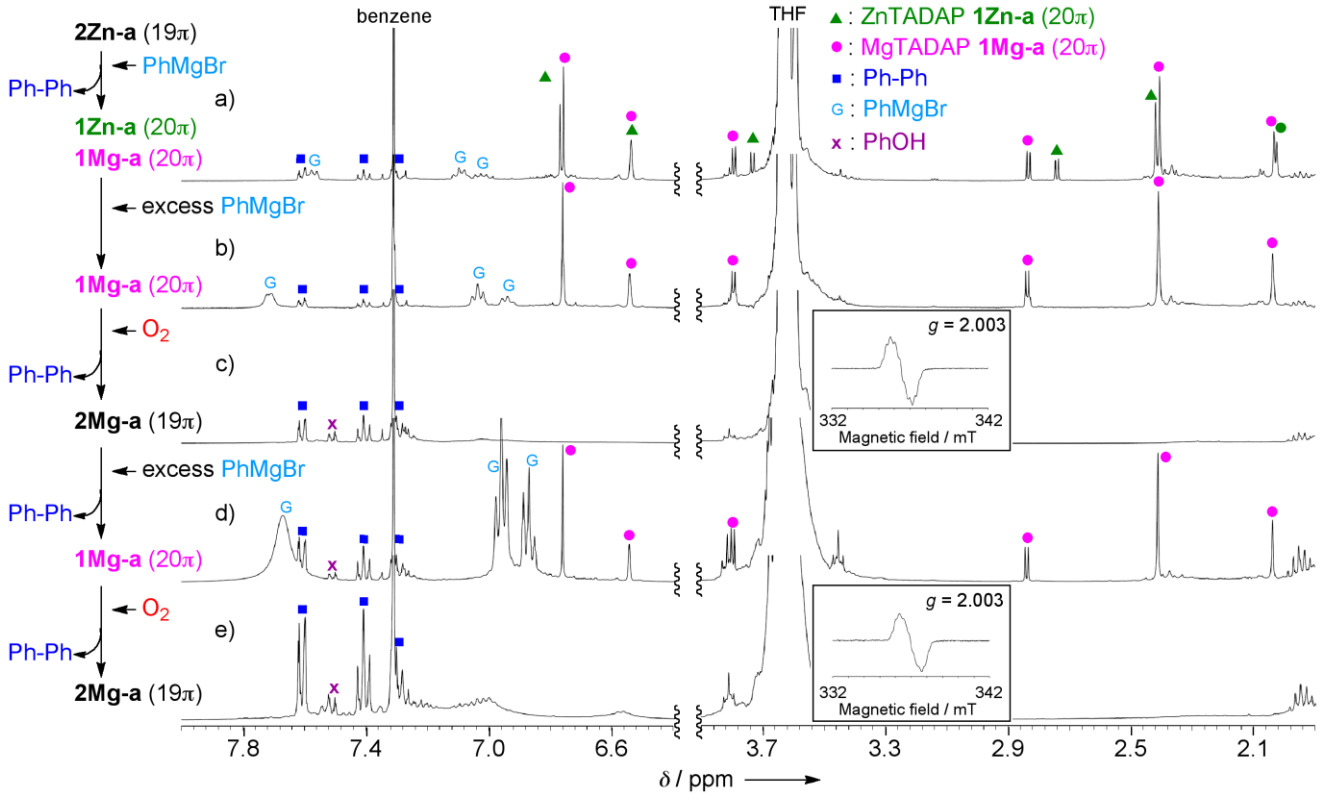

Figure 8. ^{1}H NMR and EPR spectra to follow the catalytic behavior of MTADAP in oxidative homo-coupling of PhMgBr in [D_8]THF.

Encouraged by this result, we also examined the oxidative homo-coupling of 2-naphthylmagnesium bromide in the presence of 1 mol% of **2Zn-a** in THF. As expected, 2,2'-binaphthyl was obtained in 31% yield after 6 h, where the catalytic turn-over number was 31 (for details, see SI). Although there is ample room for improving the catalyst efficiency,[32] this is the first demonstration of diazaporphyrin as a redox-active catalyst in a C–C bond-forming redox reaction of organometallic reagents.

Conclusion

We investigated the synthesis and aromatic, optical, electrochemical, and magnetic properties of TADAPs in the three different oxidation states, 20π, 19π, and 18π. The metal-templated annulation method was effective for synthesizing the zinc(II) and copper(II) complexes, and the metal–exchange reaction was used to synthesize the free base. The redox potentials and chemical stabilities of the MTADAPs strongly depend on the central metals. The nickel(II) and copper(II) complexes are more resistant to oxidation than the zinc(II) counterparts, reflecting the difference in their electronegativities. Because of the high electron affinity and resonance effects of nitrogen at the *meso* positions, the 20π and 19π derivatives resist air oxidation, while the 18π derivatives exhibit strong electron-accepting properties, compared with the isoelectronic TPP derivatives. In particular, the 19π TADAP radical cations are extremely stable towards dioxygen, moisture, and silica gel, irrespective of the central metal atom. This stability is because the unshared electron spin can be efficiently delocalized in the cationic π-system. The antiaromatic and aromatic characters of 20π and 18π TADAPs, respectively, were confirmed by NMR spectroscopy and DFT calculations. These three π-systems show quite different optical properties; their absorption bands range from 500 to 900 nm, reflecting their orbital characteristics. It is noteworthy that the redox processes among the 20π-, 19π-, and 18π-systems proceed reversibly in one-electron steps. We have established an alternative approach, the *meso* modification with nitrogen atoms, to intrinsically stabilize 20π and 19π porphyrin rings without introducing any specific central metals or peripheral substituents. TADAPs can be used not only for the fundamental study of π-conjugated azamacrocycles, but also for applied research on redox-active catalysts. This is demonstrated by the preliminary results on the oxidative homo-coupling reactions of organomagnesium compounds. The demonstrated reaction is the first example showing that diazaporphyrin acts as a redox-active catalyst in a C–C bond-forming reaction of organometallic reagents. Further studies on developing new *meso*-modified azaporphyrinoids are underway.

Experimental Section

General Remarks. All melting points were recorded on a micro melting point apparatus and are uncorrected. NMR spectra were recorded on 700 MHz (Agilent) and/or 400 MHz (Agilent or JEOL JNM-ECP) spectrometers. The ^{1}H and ^{13}C chemical shifts are reported in ppm as relative values vs. tetramethylsilane (in $CDCl_3$ and CD_2Cl_2) or a solvent residual signal (δ_H 7.16 ppm in C_6D_6), and the ^{31}P chemical shifts are reported in ppm vs. H_3PO_4. High-resolution mass (HRMS) spectra were

measured on a Thermo Fisher Scientific EXACTIVE spectrometer (electron spray–quadrupole), and MALDI-TOF mass spectra were recorded on a BRUKER AUTOFLEX III mass spectrometer. UV/Vis/NIR absorption spectra were measured on a JASCO V-530 spectrometer in the range of 300–1100 nm. The IR spectra were obtained on a PerkinElmer Spectrum GX spectrometer using KBr pellets. Electrochemical redox potentials were measured using a glassy carbon working electrode, a platinum wire counter electrode, and an Ag/Ag^+ [0.01 M $AgNO_3$, 0.1 M Bu_4NPF_6 (MeCN)] reference electrode. UV-vis fluorescence spectra were measured on an FP-8300 spectrometer. Fluorescence quantum yields were measured on a Hamamatsu Photonics Quantaurus-QY spectrometer. Thin-layer chromatography was performed with Kieselgel 60 F254, and preparative column chromatography was performed using Silica Gel 60 spherical, neutrality. All reactions were performed under an argon or nitrogen atmosphere unless otherwise noted. For the experimental details and characterization data of new compounds are reported in the Supporting Information.

Acknowledgements

This work was supported by JSPS KAKENHI (15H00931 to YM, 24109008, 15K05663 to KF, 15H00962 to MM, and 15K05392 to HN) and the Naito Foundation (YM).

Keywords: porphyrinoids • redox chemistry • dyes/pigments • aromaticity • EPR spectroscopy

[1] 16π porphyrins: a) Y. Yamamoto, A. Yamamoto, S.-y. Furuta, M. Horie, M. Kodama, W. Sato, K.-y. Akiba, S. Tsuzuki, T. Uchimaru, D. Hashizume, F. Iwasaki, *J. Am. Chem. Soc.* **2005**, *127*, 14540–14541; b) J. A. Cissell, T. P. Vaid, G. P. A. Yap, *Org. Lett.* **2006**, *8*, 2401–2404; c) Y. Yamamoto, Y. Hirata, M. Kodama, T. Yamaguchi, S. Matsukawa, K. Akiba, D. Hashizume, F. Iwasaki, A. Muranaka, M. Uchiyama, P. Chen, K. M. Kadish, N. Kobayashi, *J. Am. Chem. Soc*. **2010**, *132*, 12627–12638; d) T. Kakui, S. Sugawara, Y. Hirata, S. Kojima, Y. Yamamoto, *Chem. Eur. J*. **2011**, *17*, 7768–7771; e) S. Sugawara, M. Kodama, Y. Hirata, S. Kojima, Y. Yamamoto, *J. Porphyrins Phthalocyanines* **2011**, *15*, 1326–1334; f) S. Hiramatsu, S. Sugawara, S. Kojima, Y. Yamamoto, *J. Porphyrins Phthalocyanines* **2013**, *17*, 1183–1187.

[2] 20π porphyrin dianions: a) G. L. Closs, L. E. Closs, *J. Am. Chem. Soc.* **1963**, *85*, 818–819; b) J. W. Buchler, L. Puppe, *Liebigs Ann. Chem*. **1970**, *740*, 142–163; c) G. N. Sinyakov**,** A. M. Shul'ga, I. V. Filatov, G. P. Gurinovich, *Theor. Exp. Chem.* **1988**, *24*, 37–44; d) R. Cosmo, C. Kautz, K. Meerholz, J. Heinze, K. Müllen, *Angew. Chem. Int. Ed. Engl.* **1989**, *28*, 604–607; *Angew. Chem.* **1989**, *101*, 638–640; e) K. M. Kadish, E. Van Caemelbecke, G. Royal, in *The Porphyrin Handbook Vol 8* (Eds.: K. M. Kadish, K. M. Smith, R. Guilard), Academic Press, San Diego, **2000**, pp 1–114; f) K. Reddy, A. Basavarajappa, M. D. Ambhore, V. G. Anand, *Chem. Rev.* **2017**, *117*, 3420–3443, and references therein.

[3] M. Pohl, H. Schmickler, J. Lex, E. Vogel, *Angew. Chem. Int. Ed. Engl.* **1991**, *30*, 1693–1697; *Angew. Chem.* **1991**, *103*, 1737–1741.

[4] a) J. Setsune, K. Kashihara, K. Wada, H. Shinozaki, *Chem. Lett.* **1999**, *28*, 847–875; b) T. P. Vaid, *J. Am. Chem. Soc*. **2011**, *133*, 15838–15841.

[5] a) J. S. Reddy, V. G. Anand, *J. Am. Chem. Soc.* **2008**, *130*, 3718–3719; b) B. K. Reddy, S. C. Gadekar, V. G. Anand, *J. Am. Chem. Soc.* **2015**, *51*, 8276–8279.

[6] M. Kon-no, J. Mack, N. Kobayashi, M. Suenaga, K. Yoza, T. Shinmyozu, *Chem. Eur. J.* **2012**, *18*, 13361−13371.

[7] S. P. Panchal, S. C. Gadekar, V. G. Anand, *Angew. Chem. Int. Ed.* **2016**, *55*, 7797–7800; *Angew. Chem.* **2016**, *128*, 7928–7931.

[8] a) T. Nakabuchi, M. Nakashima, S. Fujishige, H. Nakano, Y. Matano, H. Imahori, *J. Org. Chem.* **2010**, *75*, 375–389; b) Y. Matano, H. Nakabuchi, H. Imahori, *Pure Appl. Chem.* **2010**, *82*, 583–593.

[9] a) J. A. Cissell, T. P. Vaid, A. L. Rheingold, *J. Am. Chem. Soc*. **2005**, *127*, 12212–12213; b) J. A. Cissell, T. P. Vaid, G. P. A. Yap, *J. Am. Chem. Soc*. **2007**, *129*, 7841–7847.

[10] a) J. A. Cissell, T. P. Vaid, A. G. DiPasquale, A. L. Rheingold, *Inorg. Chem*. **2007**, *46*, 7713–7715; b) E. W. Y. Wong, C. J. Walsby, T. Storr, D. B. Leznoff, *Inorg. Chem*. **2010**, *49*, 3343–3350.

[11] a) A. Weiss, M. C. Hodgson, P. D. W. Boyd, W. Siebert, P. J. Brothers, *Chem. Eur. J.* **2007**, *13*, 5982–5993; b) P. J. Brothers, *Chem. Commun*. **2008**, 2090–2102.

[12] a) Y. Matano, T. Nakabuchi, S. Fujishige, H. Nakano, H. Imahori, *J. Am. Chem. Soc.* **2008**, *130*, 16446–16447; b) Y. Matano, H. Imahori, *Acc. Chem. Res.* **2009**, *42,* 1193–1204.

[13] C. Liu, D.-M. Shen, Q.-Y. Chen, *J. Am. Chem. Soc*. **2007**, *129*, 5814–5815.

[14] T. Yoshida, W. Zhou, T. Furuyama, D. B. Leznoff, N. Kobayashi, *J. Am. Chem. Soc*. **2015**, *137*, 9258–9261.

[15] For selected reviews, see: a) K. Ishii, N. Kobayashi, in *The Porphyrin Handbook Vol 16* (Eds.: K. M. Kadish, K. M. Smith, R. Guilard), Academic Press, San Diego, **2003**, pp. 1–42; b) J. Mack, N. Kobayashi, *Chem. Rev*. **2011**, *111*, 281–321; c) Y. Matano, *Chem. Rev*. **2017**, *117*, 3138–3191.

[16] H. Ogata, T. Fukuda, K. Nakai, Y. Fujimura, S. Neya, P. A. Stuzhin, N. Kobayashi, *Eur. J. Inorg. Chem*. **2004**, 1621−1629.

[17] a) Y. Matano, T. Shibano, H. Nakano, H. Imahori, *Chem. Eur. J.* **2012**, *18*, 6208−6216; b) Y. Matano, T. Shibano, H. Nakano, Y. Kimura, H. Imahori, *Inorg. Chem.* **2012**, *51*, 12879−12890.

[18] T. Satoh, M. Minoura, H. Nakano, K. Furukawa, Y. Matano, *Angew. Chem. Int. Ed.* **2016**, *55*, 2235–2238; *Angew. Chem.* **2016**, *128*, 2275–2278.

[19] M. Horie, Y. Hayashi, S. Yamaguchi, H. Shinokubo, *Chem. Eur. J*. **2012**, *18*, 5919−5923.

[20] A. Yamaji, H. Tsurugi, Y. Miyake, K. Mashima, H. Shinokubo, *Chem. Eur. J*. **2016**, *22*, 3956–3961.

[21] a) A. Krasovskiy, A. Tishkov, V. del Amo, H. Mayr, P. Knochel, *Angew. Chem. Int. Ed.* **2006**, *45*, 5010–5014; *Angew. Chem.* **2006**, *118*, 5132–5136; b) G. Cahiez, A. Moyeux, J. Buendia, C. Duplais, *J. Am. Chem. Soc.* **2007**, *129*, 13788–13789; c) W. Liu, A. Lei, *Tetrahedron Lett.* **2008**, *49*, 610–613; d) M. S. Maji, T. Pfeifer, A. Studer, *Angew. Chem. Int. Ed.* **2008**, *47*, 9547–9550; *Angew. Chem.* **2008**, *120*, 9690–9692; e) S.-K. Hua, Q.-P. Hu, J. Ren, B.-B. Zeng, *Synthesis* **2013**, *45*, 518-526; f) T. Amaya, R. Suzuki, T. Hirao, *Chem. Eur. J.* **2014**, *20*, 653–656; g) T. Korenaga, K. Nitatori, H. Muraoka, S. Ogawa, K. Shimada, *Org. Lett.* **2015**, *17*, 5500–5503; h) S. Murarka, J. Möbus, G. Erker, C. Mück-Lichtenfeld, A. Studer, *Org. Biomol. Chem.* **2015**, *13*, 2762–2767; i) T. Amaya, R. Suzuki, T. Hirao, *Chem. Commun.* **2016**, *52*, 7790–7793.

[22] K. Murakami, Y. Yamamoto, H. Yorimitsu, A. Osuka, *Chem. Eur. J.* **2013**, *19*, 9123–9126.

[23] The diffraction data for several crystals of **2M** and **3M** (M = Zn, Cu) indicated that their DAP rings are highly flat, although these data could not be fully refined to a publishable level because of uncertain loss or positional disorder of the solvent molecules included.

[24] B. J. Littler, Y. Ciringh, J. S. Lindsey, *J. Org. Chem*. **1999**, *64*, 2864–2872.

[25] P. von R. Schleyer, C. Maerker, A. Dransfeld, H. Jiao, N. J. R. van Eikema Hommes, *J. Am. Chem. Soc.* **1996**, *118*, 6317–6318.

[26] S. P. Greiner, D. L. Rowlands, R. W. Kreilick, *J. Phys. Chem*. **1992**, *96*, 9132–9139.

[27] Y. Matano, D. Fujii, T. Shibano, K. Furukawa, T. Higashino, H. Nakano, H. Imahori, *Chem. Eur. J.* **2014**, *20*, 3342−3349.

[28] No X- and W-band EPR signals were observed for **2Cu-a** at room temperature and 20 K, respectively, probably because the large zero-field splitting interaction between the d^9 copper center and TADAP π-radical induced the significant line-broadening. In addition, no NMR signal was observed for **2Cu-a** at room temperature, which may suggest contribution of the triplet ground state. However, the detailed discussion on the spin state of 19π CuTADAP is beyond the scope of the present paper, and will be reported elsewhere.

[29] T. Ramnial, S. A. Taylor, J. A. C. Clyburne, C. J. Walsby, *Chem. Commun.* **2007**, 2066–2068.

[30] In the case of 1,4-benzoquinone as a typical two-electron oxidant, the oxidative coupling product of PhMgBr is not obtained in THF. Instead, PhMgBr attacks to the carbonyl groups to give 1,2-addition adduct. See ref. H. G. Richey, Jr, *Grignard Reagents: New Developments*, John Wiley & Sons Inc., New York, 2000.

[31] The mechanism of the reaction is not clear at present. According to the previous reports,[21a,h] the homo-coupling reaction may take place based on the stepwise electron transfer as follows: 1) electron transfer from PhMgBr to **2Mg-a** (or **2Zn-a**) (19π) to form a kind of phenyl radical species, 2) addition of PhMgBr to the radical species to give Ph-Ph radical anion species, and 3) electron transfer from the radical anion species to another **2Mg-a** (or **2Zn-a**) (19π) to afford Ph-Ph.

[32] The MALDI-TOF-MS spectrum of the crude mixture in the ^{1}H NMR experiments shown in Figure 8 indicated the formation of a small amount of the adduct of Grignard reagent to TADAP although the main peak exhibited the desired 19π MgTADAP **2Mg-a**. This might cause a decrease of the catalyst efficiency.

10.1002/chem.201703664

WILEY-VCH

Entry for the Table of Contents

FULL PAPER

A series of redox-switchable 20π, 19π, and 18π 5,10,15,20-tetraaryl-5,15-diazaporphyrinoids (TADAPs) were prepared. The aromatic, optical, electrochemical, and magnetic properties of TADAPs are strongly dependent on the oxidation states of their π-systems. MgTADAP behaved as the redox-active catalyst in a C–C bond-forming reaction of organometallic reagents.

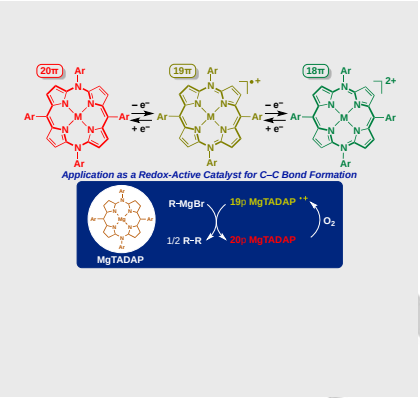

Keisuke Sudoh, Takaharu Satoh, Toru Amaya, Ko Furukawa,* Mao Minoura, Haruyuki Nakano, and Yoshihiro Matano**

Page No. – Page No.

Syntheses, Properties, and Catalytic Activities of Metal(II) Complexes and Free Bases of Redox-Switchable 20π, 19π, and 18π 5,10,15,20-Tetraaryl-5,15-diazaporphyrinoids